THE ASTROPHYSICAL JOURNAL, 388:242–252, 1992 April 1

A BOLOMETRIC MILLIMETER-WAVE SYSTEM FOR OBSERVATIONS OF ANISOTROPY IN THE COSMIC MICROWAVE BACKGROUND RADIATION ON MEDIUM ANGULAR SCALES

M. L. FISCHER,[1] D. C. ALSOP,[1] E. S. CHENG,[3] A. C. CLAPP,[1] D. A. COTTINGHAM,[1]
J. O. GUNDERSEN,[2] T. C. KOCH,[2] E. KREYSA,[4] P. R. MEINHOLD,[2] A. E. LANGE,[1]
P. M. LUBIN,[2] P. L. RICHARDS,[1] AND G. F. SMOOT[1]
Received 1991 August 8; accepted 1991 October 7

ABSTRACT

We report the performance of a bolometric system designed to measure the anisotropy of the cosmic microwave background (CMB) radiation on angular scales from 0°.3 to 3°. The system represents a collaborative effort combining a low-background 1 m diameter balloon-borne telescope with new multimode feed optics, a beam modulation mechanism with high stability, and a four-channel bolometric receiver with passbands centered near frequencies of 3 (90), 6 (180), 9 (270), and 12 (360) cm^{-1} (GHz). The telescope has been flown three times with the bolometric receiver and has demonstrated detector noise limited performance capable of reaching sensitivity levels of $\Delta T/T_{CMB} \approx 10^{-5}$ with detectors operated at $T = 0.3$ K.

Subject headings: cosmic microwave background — instrumentation: photometers

1. INTRODUCTION

Measurements of the spectrum and isotropy of the cosmic microwave background (CMB) probe the evolution and homogeneity of the early universe. The spectrum of the CMB is consistent with a blackbody with a temperature of 2.735 ± 0.06 K at frequencies from 1 to 20 cm^{-1} (Mather et al. 1990; Gush, Halpern, & Wishnow 1990). Measurements of the isotropy of the CMB have found only a dipole component to the brightness distribution. Present upper limits to anisotropy on angular scales from arcminutes to the quadrupole are in the range of $\Delta T/T_{CMB} \leq 1\text{–}5 \times 10^{-5}$ (Boughn et al. 1992; Meinhold & Lubin 1991; Meyer, Cheng, & Page 1991; Readhead et al. 1989; Smooth et al. 1991). The observed isotropy of the CMB contrasts with the abundant structure seen at optical wavelengths. Measurements of the CMB anisotropy provide one of the few critical tests of theoretical models of the formation of this structure in the early universe (Bond 1989). The angular scale of an anisotropy seen today can be related to the distance scale of the perturbation that generated it in the past. Angular scales from 10′ to several degrees cover a range of distance scales from clusters of galaxies to beyond the largest structures seen in the universe today.

Experiments searching for CMB anisotropy have been steadily improving. New detector technologies already provide the necessary sensitivity to search for anisotropy below $\Delta T/T_{CMB} = 10^{-5}$. Instruments designed to utilize these detectors must provide stable, low-background environments with excellent rejection of radiation from the Earth, and from anthropogenic radio frequency interference. In addition both thermal and nonthermal sources of emission in our Galaxy must be identified and either shown to be negligible or subtracted. Finally, compact extragalactic objects provide yet another layer of anisotropic emission which must also be understood and accounted for. The choice of measurement frequency is not critical for most types of cosmology, but has a dramatic effect on apparatus, observation strategies, and the amount of noncosmological background.

We have developed a bolometric receiver and multimode optics which fly on an existing (Meinhold & Lubin 1991) balloon-borne telescope to simultaneously measure the anisotropy in the CMB in four millimeter wavelength bands on angular scales from 0°.3–3°. The scientific results from the first two flights of the bolometric receiver are described by Fischer et al. (1991) and Alsop et al. (1992a, b). There are several reasons for this design. First, simultaneous measurements of the sky at several frequencies are necessary in order to identify the spectrum of any anisotropic emission that is detected. Second, millimeter wavelengths minimize galactic confusion and allow the use of sensitive bolometric detectors. Third, careful placement of the individual bands can provide adequately low atmospheric emission at balloon altitudes. Fourth, balloon-borne experiments at millimeter wavelengths on these angular scales can use ~ 1 m diameter antennas. These measurements complement the large angular scale experiments conducted from spacecraft such as *COBE* and *RELICT*.

The relative brightness of the CMB and the competing sources of emission determine the range of frequency which provides the best opportunity for measurement of CMB anisotropy. The brightness of the 2.735 CMB and an anisotropy in the CMB of $\Delta T/T = 10^{-5}$ are shown in Figure 1. From near millimeter to submillimeter wavelengths the dominant source of astrophysical confusion is likely to be thermal emission from interstellar dust (ISD) in our Galaxy. The curve labeled ISD in Figure 1 is an estimate of the average brightness of ISD at high Galactic latitudes based on measurements from the *IRAS* satellite at 100 cm^{-1}, and balloon-borne measurements at millimeter to submillimeter wavelengths (Hauser et al. 1984; Page, Cheng, & Meyer 1990; Meinhold & Lubin 1991). The ISD spectrum assumes a dust temperature of 22 K and an emissivity $\epsilon \propto \nu^{1.5}$, where ν is the frequency. The curve labeled Synchrotron in Figure 1 (which has a slope of $\nu^{0.1}$) is an estimate of the average brightness of synchrotron emission at high

[1] Department of Physics and Space Sciences Laboratory, University of California at Berkeley, Berkeley, CA 94720.
[2] Department of Physics, University of California at Santa Barbara, Santa Barbara, CA 93106.
[3] NASA Goddard Space Flight Center, Code 685, Greenbelt, MD 20771.
[4] Max-Planck-Institut für Radioastronomie, Auf dem Hügel 69, D-5300 Bonn, Germany.

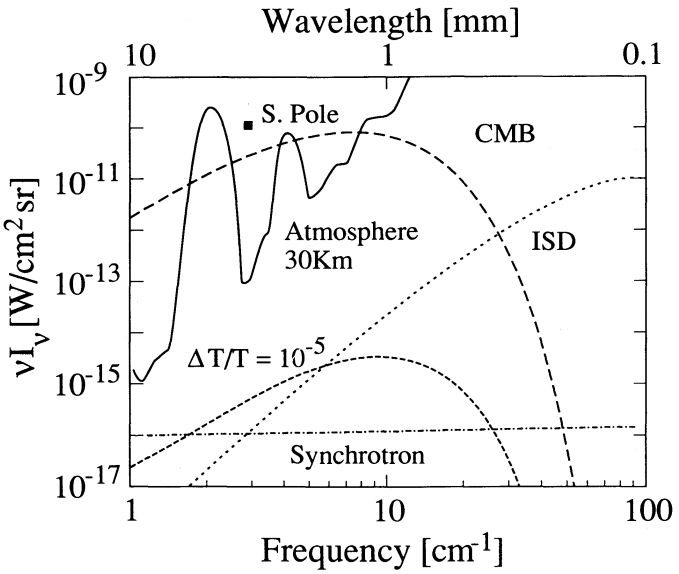

FIG. 1.—Estimates of the diffuse brightness of emission sources important for a balloon-borne anisotropy experiment at frequencies from 1 to 100 cm^{-1}. The curves include: the cosmic microwave background (CMB), an anisotropy in the CMB at the $\Delta T/T = 10^{-5}$ level ($\Delta T/T = 10^{-5}$), thermal emission from interstellar dust (ISD), galactic synchrotron radiation ("Synchrotron"), and atmospheric emission at an altitude of 30 km (Atmosphere 30 km). The point marked "S. Pole" is an estimate of the atmospheric emission from the ground at the south pole in the 3 cm^{-1} (90 GHz) window. The galactic emission curves are calculated for Galactic latitudes above 40°. The atmosphere is calculated for an observation at an elevation angle of 45°.

Galactic latitudes (Weiss 1980). At frequencies much below 3 cm^{-1} (90 GHz), nonthermal synchrotron and bremsstrahlung emission will become the dominant sources of competing Galactic emission. Typical contrast in the galactic components is less than 0.1, so these curves represent upper limits to anisotropic emission.

Atmospheric emission is a source of added background loading and noise for all but satellite experiments. The atmospheric emission for a typical balloon altitude of 30 km is shown in Figure 1. This curve is calculated for an elevation angle of 45°, using a standard atmospheric model (Goody 1964; Woody 1975) smoothed by a Gaussian filter with a constant fractional bandwidth of 0.15. For comparison, the point labeled "S. Pole" in Figure 1 is the measured atmospheric emission at the south pole in the atmospheric window at a frequency of 3 cm^{-1} (90 GHz).

Simultaneous multiband response is essential to unambiguously identify a CMB anisotropy in the presence of other sources of emission with different spectral and temporal signatures. We have designed a dichroic filterband photometer which provides these qualities by dividing the radiation collected from the same spot on the sky into several frequency bands. The centers and widths of four bands were designed to maximize the ratio of CMB anisotropy signal to atmospheric emission. The model filter used in the calculation is characterized by a flat inband response, a step function cutoff at low frequencies, and a Gaussian roll off with a fractional width of 0.05 at high frequencies. The center frequencies of these bands are 3.0, 5.8, 8.9, and 12.8 cm^{-1}, with fractional bandwidths of 0.33, 0.43, 0.40, and 0.35, respectively. These bands will be referred to as the 3, 6, 9, and 12 cm^{-1} bands.

2. INSTRUMENT REQUIREMENTS

Measurements of the anisotropy in the CMB require sensitive observations of very low contrast spatial features with a unique spectrum, in the presence of emission sources with different spectra. The requirements for a successful instrument include a stable modulation scheme for comparing the brightness of different patches of sky, a telescope with low sidelobe response and low emissivity optics, a sensitive receiver with adequate spectral resolution to discern the spectrum of any observed signal, and set of diagnostic measurements which are sensitive to a wide range of possible systematic effects. Each of these issues is discussed briefly below.

In order to maximize the sensitivity of our measurement to anisotropic signals in the presence of a much larger uniform background we chop the azimuthal position of the telescope beam by several beamwidths on the sky and detect only the signal which is synchronous with the chop. The ~6 Hz chopping frequency is high enough to avoid low-frequency noise and low enough for sensitive bolometric response. Signals at the chopping frequency that arise from sources other than the CMB and have a slowly varying amplitude will be called offsets. The chopped telescope beam is repetitively stepped or scanned in azimuth to observe a limited region of the sky. This second level of modulation will be referred to as a scan. The advantage of the periodic scan is that true sky signals will appear at specific harmonics of the scan frequency. Offsets which change more slowly than a given harmonic can be removed from the data without loss of information about the sky on angular scales corresponding to that harmonic.

Emission from the Earth which is accepted in the sidelobe response of the telescope can cause offset signals. The sidelobe response must be small enough that temperature variations in the Earth's brightness do not produce changing offsets than are large compared to an anisotropy in the CMB. A worst-case estimate of the required sidelobe response can be made by assuming that all of the radiation from the Earth is modulated by the chop. The ratio of a 30 μK CMB anisotropy ($\Delta T/T = 10^{-5}$ at 6 cm^{-1}) accepted in the $\sim 10^{-4}$ sr solid angle of the main telescope beam to 300 K Earth radiation accepted in a solid angle of 2π sr is $\sim 2 \times 10^{-12}$. This ratio would suggest that -120 dB rejection is required. In fact, the required rejection is unlikely to be this stringent. An accurate estimate of the required sidelobe response depends on the spatial structure in the Earth's brightness and on the two-dimensional telescope sidelobe response. Unfortunately, both of these quantities are very difficult to estimate. In the design discussed below, control of the sidelobe response is accomplished with an off-axis optical design, oversized mirror surfaces, and baffles which prevent Earthshine from directly illuminating the mirror surfaces.

Thermal emission from the telescope optics is a source of photon noise and a potential source of offset signal. The brightness of the emission from the mirrors will depend upon the temperature and emissivity of the mirror surfaces. In the balloon-borne environment, the optics temperatures approach the 220 K temperature of the ambient air. At millimeter wavelengths, the emissivity of a metal surface $\epsilon \propto (\nu/\sigma)^{1/2}$, where ν is the frequency, and σ is the DC electrical conductivity. For smooth pure aluminum $\epsilon = 10^{-3}$ at 3 cm^{-1} (90 GHz) and $T = 220$ K. A mirror surface machined in an aluminum alloy has a somewhat higher emissivity. Optics with an emissivity of 2×10^{-3} at 220 K will be from 0.4 to 6 times as bright as the

CMB at frequencies from 3 to 10 cm^{-1}. Variations in the temperature of the mirror surfaces can generate offset signals if the illumination of the mirrors changes synchronously with the chop. Changes in the offsets due to changes in the mirror illumination or drifts in the mirror temperature must remain small compared to an anisotropy in the CMB on the time scale of a scan. In the design described below, changes in the detector offsets due to chopped mirror emission and beam spillover at the mirror edges are minimized by the use of an extremely stable mechanical system to chop the telescope beam. The temperatures of all of the optical elements are also measured during flight.

3. DESCRIPTION OF THE INSTRUMENT

The instrument which we have developed to meet the requirements discussed above is based on a balloon-borne telescope originally designed to search for CMB anisotropy with a heterodyne receiver (Meinhold & Lubin 1991). A paper by Meinhold et al. (1992) gives a complete description of the original telescope optics, the receiver, the balloon gondola, and the telescope pointing system. This section describes the new multimode optical design, the secondary mirror chopper drive, the in-flight calibration, the four-band photometer, the cryostat, and the receiver electronics.

3.1. *Optics*

The optical system is the off-axis Gregorian telescope shown in Figure 2. A large secondary mirror and a cooled, broadband feedhorn have been developed to accept multiple electromagnetic modes in a 0°.5 FWHM field of view at frequencies from 2.5 to 15 cm^{-1}. This section describes the optical layout and the method used to chop the beam on the sky, the details of the fabrication of the mirrors, the design and fabrication of the feedhorn, and the measured beam patterns of the feedhorn and the complete telescope.

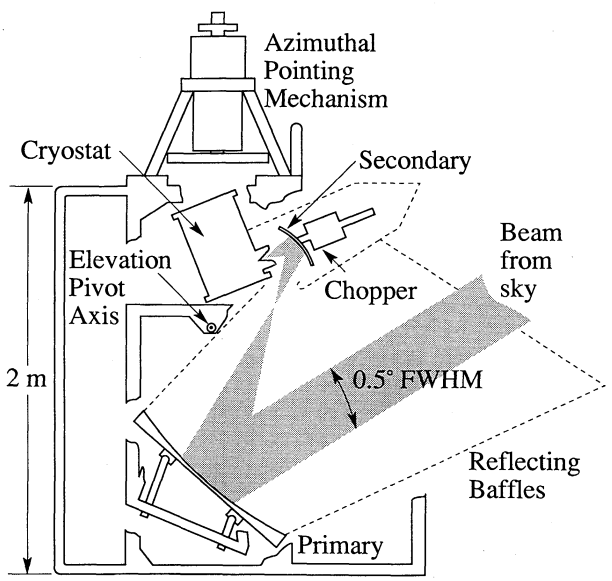

FIG. 2.—Sideview of the gondola with the outer frame cut away to expose the inner frame holding the optical system and the detector cryostat. The gondola is pointed using the azimuth reaction wheel mounted on the top of the outer frame and by rotating the inner frame in elevation. The shaded region indicates the −3 dB contours of illumination on the mirror surfaces. The dashed lines indicate reflecting baffles which prevent Earthshine from directly illuminating the optical surfaces.

The primary mirror is a f/1.0 off-axis section of a paraboloid with a focal length $L = 1$ meter and an off axis angle of 38°. The secondary mirror is an off axis section of an ellipsoid of revolution. The lines that connect the secondary focus and the primary focus to the center of the secondary mirror have lengths $L_1 = 24.8$ cm and $L_2 = 33.0$ cm, respectively, and the angle between them is $\eta = 45°$. The edge of the secondary mirror is defined by the intersection of a circular cone which has a 53° full angle with the ellipsoidal surface. The cone is centered on the feedhorn axis with its apex at the secondary mirror focus. The secondary mirror is positioned so that the prime focus of the telescope is reimaged in the feedhorn at the X marked on Figure 3.

The position of the telescope beam on the sky is chopped in azimuth by rotating the secondary mirror through a small angle about the optical axis of the feedhorn. This rotation displaces the image of the feedhorn away from the prime focus of the telescope. The angular displacement of the telescope beam on the sky $\Delta\theta_{sky} = \Delta\phi \sin \eta(L_2/L) = 0.24\Delta\phi$, where $\Delta\phi$ is the angular rotation of the secondary mirror. Since the beam pattern of the feedhorn is axially symmetric, this method of chopping combined with the design of the secondary mirror edge, maintains a constant illumination on the secondary mirror and minimizes chopped spillover at the edge of the secondary mirror. The beam position on the primary mirror is chopped which places requirements on the stability of the chopper drive which will be addressed below.

The primary mirror surface was fabricated at Bell Laboratories for the Lubin, Meinhold, & Chingcuanco (1990) experiment. It was machined from a cast aluminum plate on an NC milling machine using a 15 cm diameter ball end mill and then lightly polished by hand. The machining grooves are visible with a spacing of ~4 mm. The back of the mirror was machined to provide a stiff lightweight support structure. The total mirror weight is ~40 kg.

The surface of the secondary mirror was cut in 6061-T6 aluminum on a NC milling machine using a 5 cm diameter ball end mill. The mirror surface was carefully polished by hand to remove the machining grooves. After the mirror surface was machined and polished, the back of the mirror was thinned to a thickness of 6 mm on a lathe. The mirror was balanced statistically and dynamically about the rotation axis by adding a counterweight on the back. The weight of the finished mirror is 1.3 kg. The moment of inertia about the rotation axis is ~80 kg cm^2.

The feedhorn is an off-axis parabolic concentrator (Winston cone) with a constant radius flare to reduce the acceptance of radiation from large angles shown in Figure 3 (Mather 1981; Santo et al. 1987). The concentrator defines a 14° FWHM geometric beam and a throughput of 0.126 cm^2 sr (Winston 1970). The flare has a radius of curvature of 7 cm which extends to an angle of 45° from the horn axis and a 3 mm radius lip which extends to 90° from the horn axis. Since the flare is long compared to the concentrator the geometric beam is further limited to 12° FWHM. The horn will accept ~1, 4, 9, and 16 modes in the 3, 6, 9, and 12 cm^{-1} bands, respectively.

The feedhorn was electroformed on a gold plated aluminum mandrel which had been shaped on a numerically controlled (NC) lathe and polished by hand. The copper body was then machined and the aluminum mandrel was then etched away. The outer surface of the finished feedborn was coated with an evaporated gold layer to reduce its emissivity.

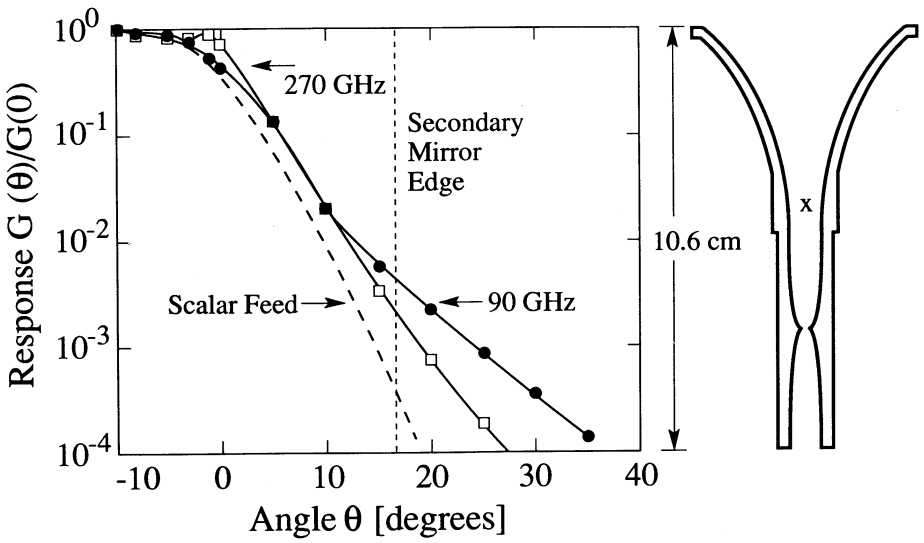

FIG. 3.—Feedhorn cross section and measured beam pattern. The cross section shows the smooth walled collimating cone and long radius apodizing flare. The location of the secondary focus is marked with an "X." The beam pattern measurements show the angular response at 3 cm^{-1} (90 GHz) and 9 cm^{-1} (270 GHz). The vertical line indicates the angle subtended by the edge of the secondary mirror. The dashed curve shows the theoretical response of a scalar feedhorn with the same FWHM response for 90 GHz.

Two upward-looking scoop-shaped baffles were employed to prevent Earthshine and radio frequency power (RF) from directly illuminating the feedhorn or the mirror surfaces (Fig. 2). The first baffle surrounds the primary mirror, and the second baffle surrounds the secondary mirror, the chopper drive, and the cryostat. The baffles were made of sheet aluminum; the seams were sealed with metallic RF tape. The final tests of the beam pattern were made with the baffles in place.

The beam pattern of the feedhorn shown in Figure 3 was measured at frequencies of 3.0 cm^{-1} (90 GHz), and 9.0 cm^{-1} (270 GHz) using a microwave oscillator and a harmonic generator as the radiation source. Both patterns show a well-defined main lobe and exponentially attenuated sidelobes that are a characteristic of the apodizing flare. The measured amplitude and shape of the sidelobes are in good agreement with calculations using the geometrical theory of diffraction (Mather 1981). For comparison we also show the beam pattern expected for a scalar feedhorn with the same FWHM beam size which operates over a 50% bandwidth near 90 GHz. The broad bandwidth of our feedhorn is achieved at a significant cost in the sidelobe response. This disadvantage of our dichroic system is partly compensated for by the large diameter of the secondary mirror. The measured beam pattern has been used to estimate that from 0.01 to 0.02 of the system throughput is accepted from angles beyond the edge of the secondary mirror in the four passbands. Most of this throughput is either filled by the sky or is redirected upward by the secondary mirror baffle to the sky. A small fraction is filled by the balloon, and the gondola rigging when observations are made at an elevation between 30° and 40°.

The beam pattern of the complete telescope shown in Figure 4 was measured at frequencies of 3.0 cm^{-1}, and 9.0 cm^{-1} using the same coherent radiation source as above. The telescope was located on the ground in a large open space, the source was on the roof of a 15 m high building that was 50 m away. The beam pattern was measured by scanning the telescope elevation from 15° to 55°. The main beam of the 3.0 cm^{-1} pattern is ~Gaussian with a width of 0°.5 FWHM. The main beam at 9 cm^{-1} has the same FWHM size, but has more structure, which is probably due to standing wave resonances. The far sidelobes of the 3 cm^{-1} pattern were measured in a range between −70 and −80 dB at angles between 20° and 40° from the main beam. Measurements made with the secondary mirror fixed at the extrema of the normal chopping motion showed no significant change in the beam patterns. Sidelobe response at this level will allow the telescope to accept a brightness temperature of ~1 K integrated over the solid angle of the Earth. The component of this radiation that is modulated by the chop must remain stable over the time scale of the scan. The size of the chopped component depends upon the coupling between the structure in the beam pattern and the structure in the Earth's brightness. Our plans include measurements at low elevations to estimate the size of this coupling.

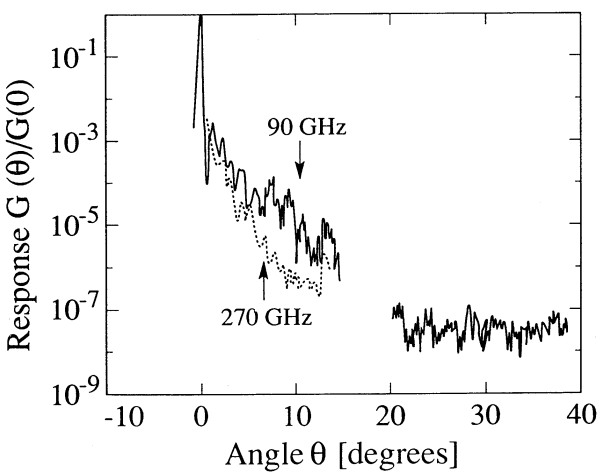

FIG. 4.—Telescope beam pattern measured as a function of elevation angle at 90 GHz (*solid line*), and 270 GHz (*dashed line*). Data for the range of angles from 16° to 20° is missing. The response shown from 20° to 40° is an optical signal but we can not exclude the possibility that it is due to low-level reflections from the ground or from buildings.

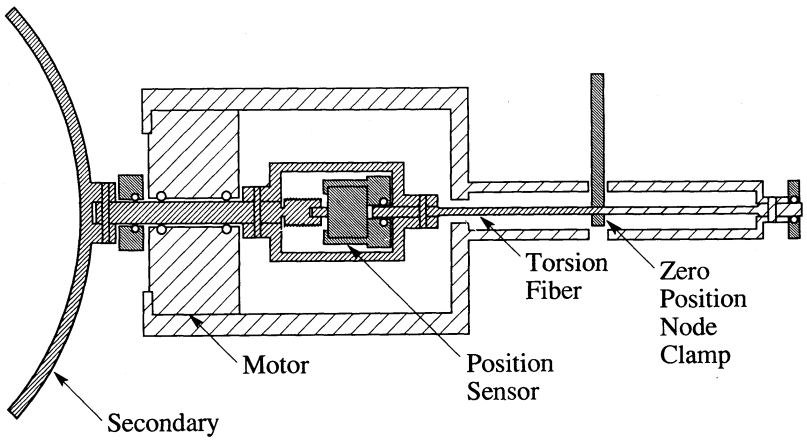

FIG. 5.—Cross-sectional view of the chopper drive as seen from above. The secondary mirror, the motor shaft, the inner yoke, and half of the length of the torsion fiber (*medium hashed regions*) rotate in opposition to the motor housing, the outer yoke, and the other half of the fiber (*coarse hashed regions*). The remaining (*fine hashed*) regions idicate the nonmoving parts of the structure which support the moving parts through ball bearings. The zero position of the mirror motion is fixed by clamping the torsion fiber at the node between the mirror and the motor.

3.2. *Secondary Mirror Chopper Drive*

The drive for the secondary mirror rotates the mirror so as to produce a sinusoidal motion of the beam on the sky. A rotation of 5.'4 gives a peak to peak chop on the sky of $\Delta\theta_{sky} = 1.'3$ *p-p*. As shown in Figure 5, the mirror is mounted on ball bearings and is coupled to a counterrotating DC servo motor by a torsion fiber which gives a resonance frequency near 6 Hz to insure that very little torque is coupled to the gondola frame. The zero position of the mirror motion is determined by clamping the torsion fiber at the stationary node between the mirror and the motor. Small adjustments to the zero position are made by moving the other end of the arm with a screw driven by a stepper motor. The amplitude and zero position of the mirror motion can be adjusted during the flight.

The position of the mirror is measured with a rotary variable differential transformer (RVDT) manufactured by Shavitz, Inc. Feedback electronics controls the motor drive from the reference signal. The electronics have two loops: one which adjusts the phase of the driven signal to keep the oscillation frequency near resonance, and a second which controls the amplitude of the mirror motion.

The fractional stability of the secondary mirror motion is defined as the ratio of the RMS stability to the standard operating amplitude of 2.'7. During laboratory tests the fractional stability is $\sim 4 \times 10^{-4}$ for the amplitude and 2×10^{-3} for the zero position. The measured signals are averaged by low-pass filters with a two-pole roll off with a time constant of 3 s and monitored on the time scale of hours. The stability in zero position and amplitude depend upon the condition of the bearings, the amplitude of the motion, the elevation of the telescope (worse at higher elevation), and the position of the node clamp. The DC change in the chopper zero position is less than 0.'02 when the telescope elevation is changed from 15° to 55°.

3.3. *Multiband Photometer*

Radiation accepted by the feedhorn is recollimated by a second parabolic concentrator to an f/2.4 beam, filtered by two low pass filters, and then enters the photometer shown in Figure 6. The photometer divides the radiation into four bands using three dichroic filters. Additional blocking filters improve the out-of-band rejection before each beam is recondensed onto a bolometric detector. The entire photometer including many of the filters, the bolometers and the load resistors, is cooled to 0.3 K by a ^{3}He refrigerator.

The first low pass filter is a 0.79 mm thick *z*-cut crystal quartz window, to absorb the near-infrared power and conduct it to the ^{4}He bath. The thickness of the quartz filter was chosen to cancel reflections in the 3 cm^{-1} band. The second filter is a 0.75 mm thick disk of black polyethylene imbedded with 100 μm diameter glass beads, which absorbs the remaining radiation from 20 cm^{-1} to the visible (Sato et al. 1989). The quartz and the glass bead filters are cooled to 2 K. The order in which the bands are divided was chosen to maximize the small signals available from the CMB at 3 cm^{-1} by transmitting the 3 cm^{-1} band first and reflecting the 6, 9, and 12 cm^{-1} bands. The dichroic filters chosen to do this are commercially available multilayer capacitive mesh lowpass filters with high-frequency cutoffs at 3.5, 7.2, and 10.5 cm^{-1} (Cochise Instruments, Inc.). The mesh parameters and layer spacing were optimized for use at normal incidence. In this dichroic application we used the filters at a 22.'5 angle of incidence. The photometer contains additional filters which improve the out-of-band rejection.

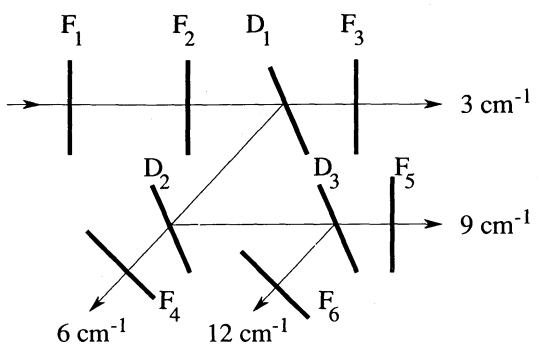

FIG. 6.—Schematic diagram of the dichroic photometer. Filter F1 represents the combination of a quartz filter which blocks near-infrared radiation and a glass bead filter which blocks from ~0.5 mm through the visible. Three dichroic mesh filters D1-D3, tipped at a 22.'5 angle of incidence divide the incoming radiation into four spectral bands. Filter F2 is a capacitive mesh low pass filter with a cutoff at 15 cm^{-1}. Filters F4–F6 are high pass filters used at a normal incidence to define the passbands. The filtered radiation is then concentrated onto bolometric detectors in passbands centered near 3, 6, 9, and 12 cm^{-1}, respectively.

These include a multilayer capacitive mesh filter with a low-pass cutoff at 15 cm^{-1} mounted at normal incidence at the photometer entrance, and "thick grill" high-pass filters made by machining close-packed arrays of circular holes in metal plate (Timusk & Richards 1981). Because of the stringent requirements for high-frequency rejection in the 3 cm^{-1} band, an additional multilayer capacitive mesh filter with a cutoff at 4 cm^{-1} was included at normal incidence.

The detectors used in this experiment are composite bolometers (Lange et al. 1983). The bolometers for the four passbands are placed in an integrating cavity at the exit aperture of a parabolic concentrator. The radiation is absorbed in a thin metal film evaporated on a dielectric substrate. The thickness of the metal film is chosen so that the surface impedance of the metal/dielectric structure is matched to free space. The substrates used in the first flight were 25 μm thick 2.5 mm squares of sapphire with a 83 Å thick Ti absorbing film. For the second flight we used diamond substrates and a 800 Å thick Bi absorbing film. In both cases resistance thermometers doped by neutron transmutation were used to measure the substrate temperature (Haller 1985).

The sensitivity of an optimized bolometer is limited by the phonon noise contribution to the noise equivalent power $NEP_{phon} = \sqrt{(4kT^2G)}$, where k is Boltzmann's constant, T is the bolometer temperature, and G is the thermal conductance of the connection between bolometer and the heat sink. When the background does not significantly heat the detector, the sensitivity can improved by reducing G until the phonon noise is equal to the Johnson noise of the thermometer. The thermal conductance of the detectors used in the first flight was dominated by the two 4 mm long 8 μm diameter brass electrical leads thermal conductance of the electrical leads to the thermometer which gave a thermal conductance $G \approx 10^{-8}$ W/K near 0.3 K. The detectors used in the second flight had 8 μm diameter graphite fiber leads which gave $G < 10^{-9}$ W/K. The thermal conductance of these detectors was dominated by the nylon threads used to support the bolometer substrate. When operated at a heat sink temperature of 0.3 K and a chopping frequency of 6 Hz these graphite fiber bolometers had an electrically measured $NEP_{elec} \approx 1.0 \times 10^{-16}$ W/$\sqrt{Hz}$, a time constant of 10 ms, and an electrically measured responsivity $S_{elect} \approx 10^8$ V/W.

The bolometers are wired in series with 20 MΩ cold load resistors and the bolometer voltages are measured with preamp circuits which have a gain of 10^4 at 5 Hz and unity gain at DC. The preamp electronics include detector bias supplies for each signal channel. A single pole in the preamp circuit rolls off the response above 50 Hz. After preamplification, the detector signals are low-pass filtered with a two-pole anti-aliasing Bessel filter with a −3 dB point at 50 Hz and a gain of 10 at DC. Since the bolometers will rectify any RF frequency, it is essential to prevent pickup from the telemetry transmitters or other sources from reaching them. The preamp electronics are mounted directly on top of the cryostat in an aluminum box which is carefully sealed with metal tape. All wires entering the preamp box are filtered with RF filters before entering the cryostat. Radial wires are connected between the lip of the feedhorn and the cryostat wall to avoid TEM mode propagation into the cryostat.

3.4. *Cryostat*

The side looking cryostat contains 4 liter liquid N_2 and ^{4}He tanks with a ^{3}He refrigerator mounted coaxially inside the cylindrical bore of the ^{4}He tank, all purchased from Infrared Systems, Inc. During flight the N_2 and ^{4}He volumes are pumped by the atmosphere to pressures near 10 Torr. The exit end of the feedhorn is clamped to the ^{4}He cold surface at a temperature near 2 K. The flared entrance to the feedhorn is heated to 3 K by ambient temperature radiation entering the cryostat. The ^{3}He refrigerator maintains the photometer temperature near 0.3 K. The entrance aperture of the cryostat is sealed by a 50 μm thick polypropylene vacuum window to minimize the emissivity of ambient temperature material in the beam. Because the polypropylene window is permeable to healing gas, a 15 μm thick polypropylene outer window is mounted on the cryostat and nitrogen gas is flowed between the windows to reduce the helium gas concentrations near the vacuum window. This procedure also reduces the probability of moisture condensation on the cool vacuum window at launch.

The ^{3}He refrigerator contains 3 STP liters of gas and has a hold time of 24 hours in the laboratory with the ^{4}He bath not pumped. Two mechanically operated heat switches are used to connect the pump and evaporator volumes to the ^{4}He tank during cycling. The photometer is mounted directly to the ^{3}He coldplate but is held in place by Kevlar cords which raise all the mechanical resonances of the photometer above 40 Hz. During the flight the temperature is monitored with a carbon thermistor.

3.5. *Inflight Calibrator*

The system responsivity is calibrated during the flight by moving a partially reflecting membrane into the antenna beam near the prime focus so that the chopper motion causes the beam to move on and off the membrane. The membrane reflects a known fraction of the radiation from an ambient temperature black flight load to the detectors as shown in Figure 7. The membrane is a 12 μm thick polypropylene film epoxied between two semicircular alluminum rings. The membrane is

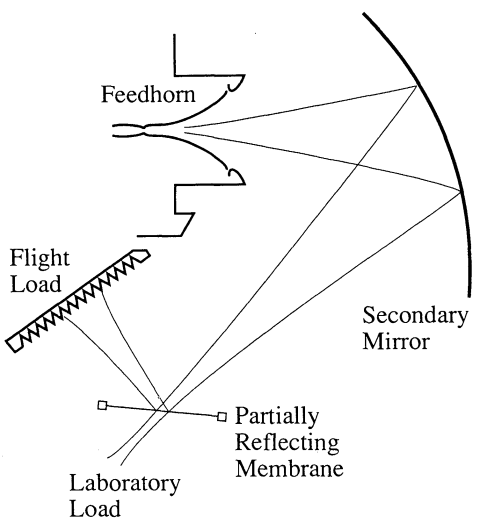

FIG. 7.—Cross-sectional view of the calibration scheme showing the reflective membrane, which fills half of the focal plane at the prime focus, the flight load, and the secondary mirror and feedhorn. The membrane reflects a known fraction (0.001–0.005) of the calibrator radiation into one lobe of the chopped beam pattern. The −3 dB contours show the filling on the optic elements. Laboratory calibration is carried out with laboratory loads located below the prime focus.

rotated into the beam on the end of an arm driven by a stepper motor under control from the ground. The membrane is moved into the beam in small steps which allows us to find the position of maximum signal. The flight load is a 1 cm thick sheet of Eccosorb which has been grooved to minimize reflections (Emerson & Cuming, Inc.).

Low-background bolometric detectors require an in-flight calibration source which does not saturate the detector response. The membrane calibrator reflects sufficient radiation to allow a high signal-to-noise measurement without affecting the operating point of the detectors. The average reflectivity of the calibrator membrane is measured in the laboratory by comparing the signals in each passband from the membrane to the signals from blackbody sources of a known temperature difference placed at the prime focus. The membrane reflectivity determined in this way increases from 10^{-3} to 10^{-2} at frequencies from 3 to 15 cm^{-1}. The emissivity of the membrane is 20–100 times smaller than the reflectivity at the frequencies, justifying the assumption of a purely reflective source.

3.6. *Electronics*

The flight electronics are divided into two separate systems. The first system, described elesewhere provides the overall gondola control and the telescope pointing (Chingcuanco 1989). The second serves the receiver, secondary mirror chopping mechanism, and ambient temperature thermometers. The receiver electronics includes preamp power, and cryogenic thermometer circuits which measure carbon resistance thermometers attached to the ^{3}He, ^{4}He, and N_2 baths, and to the open edge of the feedhorn. The chopper drive electronics includes the RVDT readout, feedback, and command control electronics described above.

The AD-590 ambient temperature thermometers from Analog Devices, Inc., are used in two modes. Single sensors measured the DC and AC components of the temperature of the preamp case, the cryostat snout, the secondary mirror chopper mechanism, the primary mirror, and the ambient air. The DC thermometers have a resolution of 0.4 K. The AC thermometers have a resolution of 10 mK, and a bandwidth from 17 mHz to 1.6 Hz. Pairs of thermometers are used to measure the temperature difference across the primary mirror and the primary mirror baffles along the direction of motion of the chopped beam. These differential measurements have a resolution of 10 mK.

The four detector channels and the chopper position reference signal are digitized in the range from -10 to $+10$ volts with a 16 bit analog to digital converter (A/D) at a frequency of 250 Hz. This high digitization speed is used to facilitate indentification and removal of spikes due to cosmic rays hitting the bolometers. The rest of the analog signals are digitized in the range from 0 to $+5$ volts with an 8 bit A/D at 31.2 Hz. The digitized analog information plus several bytes of digital information are combined into a 128 byte telemetry frame. The data are transmitted as a 32 kbit s^{-1} Bi-phase encoded serial data stream.

The receiver and gondola control electronics utilize separate FM/PM telemetry channels, at frequencies near 1.5 GHz, provided by the NSBF consolidated instrument package (CIP). In addition, a separate transmitter operating near 1.5 GHz is used to transmit pointing information from a CCD star camera. All of these antennas are mounted below the gondola on the ends of 2 m long PVC tubes to minimize their motion with respect to the telescope.

The bolometer signals and the chopper reference are reconstructed on the ground from the digital information and processed by four analog lock-in amplifiers. Chart recordings are made of the signals and of the housekeeping data for decision making purposes during the flight. The digital data are also stored separately for later analysis. During the second flight a VAX-3500 stored the data directly to hard disk and provided digital processing of the detector signals. This processing included cosmic-ray detection and blanking, and digital lock-in amplifiers phase locked to the secondary mirror motion. Commands are sent to the receiver and chopper electronics using the NSBF tone command system. The gondola control system is operated from a separate ground station which communicates with the point electronics over a 1200 baud asynchronous communications link. This requires a separate up-link transmitter operated near 500 MHz.

4. CALIBRATION OF THE INSTRUMENT

The instrument makes a differential measurement of the sky brightness in each passband by sinusoidally modulating the position of the 0°.5 FWHM Gaussian beam through an angle of 1°.3 on the sky at a frequency near 6 Hz. The digitized detector signals are demodulated by computer using a lock-in amplifier algorithm. An accurate calibration requires knowledge of the spectral response of each passband, the shape of the chopped beam pattern on the sky, and the responsivity of each band to a known calibration source.

The spectral response of the instrument was measured with a Fourier transform spectrometer. The measurement was made by illuminating the entrance aperture of the flight-ready instrument with the spectrometer output. Interferograms were collected separately for each passband and Fourier transformed to give the unnormalized spectral response. The instrumental response was normalized to that of a separate bolometric detector system which had approximately flat response to frequencies from 2 to 30 cm^{-1}. The relative instrumental response spectra are shown in Figure 8. Because the dynamic range of the spectrometer measurement is limited to approximately -25 dB, and the out-of-band response must be measured to the -40 dB level of the in band signal, the low-level, high-frequency leakage was measured separately from the main passband. The high-frequency response was measured

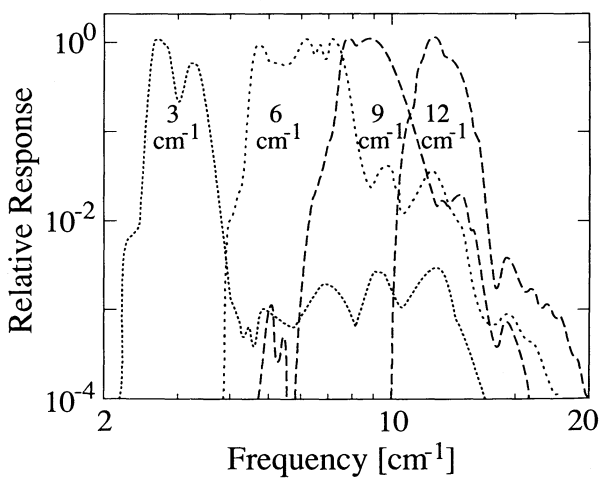

FIG. 8.—Relative spectral response of the four bands. The response of each band has been normalized to unity.

TABLE 1

INTEGRATED BRIGHTNESS OF EMISSION SOURCES[a]

Band Center (cm^{-1})	ΔP_{CMB}[b,c]	P_{ISD}[c,d]	ΔP_{R-J}[e,f]	P_{Atm}[f,g]
3.....	0.35	0.90	6.0	1.6
6.....	3.6	20	100	23
9.....	3.6	47	190	60
12.....	1.8	150	400	440

[a] Emission sources from Fig. 1 integrated over measured passbands.
[b] CMB Anisotropy of $\Delta T/T_{CMB} = 10^{-5}$.
[c] In units of 10^{-16} W cm^{-2} sr.
[d] Interstellar dust emission with $T_{dust} = 22$ K, and $\epsilon \propto \nu^{1.5}$.
[e] Raleigh-Jeans blackbody source of temperature difference $\Delta T = 1$ K.
[f] In units of 10^{-12} W cm^{-2} sr.
[g] Atmospheric emission at an altitude of 30 km, and 45° elevation.

out to 30 cm^{-1} by introducing thick grill blocking filters at the spectrometer output which were chosen to minimize the inband power for each passband. Limits to the high-frequency reponse above 30 cm^{-1} were estimated separately by measuring the integrated response above 30 cm^{-1} from a high-pass filtered blackbody source chopped in temperature between 77 and 300 K.

The measured spectral response of each passband has been used to calculate the power expected in each band from a CMB anisotropy with $\Delta T/T_{CMB} = 10^{-5}$, emission from ISD at high galactic latitudes, a blackbody source with a temperature difference of 1 K in the Raleigh-Jeans limit, and atmospheric emission at an altitude of 30 km and an elevation of 45° as is shown in Table 1. The frequency dependance of the calculated power is sufficiently different that it will be possible to discriminate between these different sources, given measurements with sufficient signal-to-noise ratio.

The chopped beam pattern depends upon the unchopped beam pattern, the shape of the chopped motion, the frequency response of the detection system, and the weighting function of the lock-in amplifier algorithm. The chopped beam pattern has been calculated assuming a 0°.5 FWHM Gaussian beam, a sinusoidal chop with an amplitude of 0°.65, a detection system with a flat frequency response, and a lock-in algorithm which uses a square wave weighting function. The chopped beam pattern, calculated with the above assumptions, closely matches the pattern measured by scanning across the planet Venus during the first flight as is shown in Figure 9.

Accurate determination of the responsivity of each passband is accomplished by measuring the signal from a calibration source which fills a known fraction of the chopped telescope beam. The primary calibration is carried out in the laboratory and then transferred to the flight by use of the membrane calibrator. The reflectivity of the membrane is measured in the laboratory with the receiver, the calibrator, and the secondary mirror in the flight configuration. A neutral density filter mounted inside the cryostat in front of the photometer transmits 0.02 of the incoming radiation which limits the background loading and signal level on the detectors. A large blackbody load cooled to 77 K is placed so as to intercept the beam which would normally be transmitted, through the membrane, to the primary mirror. The measured signal voltage from the membrane in the laboratory is

$$V_{ml} = SR_{eff}(T_{Ll} - 77\ \mathrm{K})\,, \qquad (1)$$

where S is the system responsivity in Volts/Kelvin, R is the

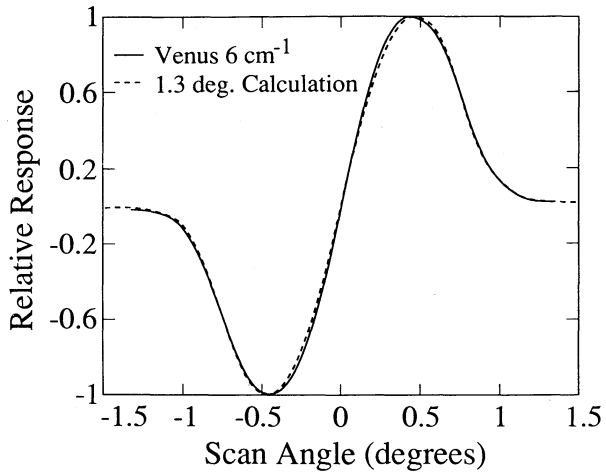

FIG. 9.—Chopped beam pattern of the telescope. The solid line shows a measurement of the chopped beam pattern made by scanning over the planet Venus. The dashed line shows the calculated response assuming a 0°.5 FWHM Gaussian beam, a 1°.3 *p-p* amplitude sinusoidal chop, flat frequency response from the detection system, and demodulation by a square wave reference.

reflectivity of the membrane, and T_{Ll} is the temperature of the flight load in the laboratory.

The responsivity S is obtained from a separate measurement by chopping the beam between two blackbody loads mounted at the prime focus and side by side along the direction of the chop. One load is held at a temperature of 273 K with an ice water bath, and the other at a temperature near 293 K with an ambient water bath. The temperatures of both loads are measured with mercury thermometers to an accuracy of ± 0.5 K. The entrance apertures of the loads are covered with a 25 μm thick polypropylene window to prevent condensation inside the loads. In order to improve the linearity of the detectors for such large signals, the electrical bias power on the bolometers is made large compared to the change in optical power between the 300 K water bath measurement and the 77 K membrane measurement. The DC electrical responsivity of each detector is measured to correct for the residual 1%–10% change in responsivity between these measurements.

The effective reflectivity of the membrane is measured several times before each flight. Because the filter bands were changed between the first and second flights by the removal of the 3.3 mm band, the reflectivities also changed. The measured membrane reflectivities are listed separately for the two flights in Table 2. The measured values are within a factor of 2 of the calculated reflectivity of a 12 μm thick dielectric film, illumi-

TABLE 2

MEMBRANE REFLECTIVITY

Band Center (cm^{-1})	Reflectivity (10^{-3})		
	1989 Nov[a]	1990 Jul[b]	Calculated[c]
3.....	1.0	(removed)	0.45
6.....	1.9	2.4	1.5
9.....	2.6	3.1	2.6
12.....	5.2	5.9	4.5

[a] Measured before first flight of 1989 November.
[b] Measured before second flight of 1990 July.
[c] Calculated reflectivity of a lossy dielectric film described in text.

nated at an angle of 45°, with the index of refraction $n = 1.5$ and the absorption coefficient $\alpha(\nu) = 0.01 + 0.05\nu$ (cm^{-1}) of polypropylene (Afsar 1987). Here ν is the frequency in cm^{-1}. These values are calculated from the nominal band centers of 3, 6, 9, and 12 cm^{-1} and are underestimates in the 3 and 6 cm^{-1} bands because the reflectivity grows steeply toward higher frequencies.

The responsivity of the system is determined during the flight by measuring the bolometer signals and the temperature of the flight load. The membrane reflectivity measured in the laboratory is then used as a transfer standard to calculate the responsivity of the system to a Rayleigh-Jeans blackbody filling one half of the sky. The measured signal on the detectors due to the membrane in flight will be

$$V_{\mathrm{mf}} = SR_{\mathrm{eff}}(T_{\mathrm{Lf}} - T_{\mathrm{sky}}) , \quad (2)$$

where T_{Lf} is the temperature of the flight load, and T_{sky} is the antenna temperature of the total background loading in each passband. The antenna temperature of the background is estimated by accounting for each of the emission sources present during the flight. The accuracy of this estimate is not critical because $T_{\mathrm{Lf}} \approx 220$ K and $T_{\mathrm{sky}} \approx 5$–10 K. A factor of 2 error in T_{sky} results in a 10% calibration error.

5. FLIGHT PERFORMANCE

The first flight was launched at 22 UT on 1989 November 15 from the National Scientific Balloon Facility (NSBF) at Fort Sumner, New Mexico. The 750 kg telescope achieved a float altitude of 29 km. The ambient pressure and temperature were ~15 Torr and ~210 K, which are typical of that altitude. Observations made over a period of 10 hours at float altitude, included scans of Venus and Jupiter, four scans of the Galactic plane, and a 40 minute search for anisotropy in the CMB near the north celestial pole. Tests were also made for systematic sources of noise in the demodulated detector signals.

The noise in the detector signals was consistent with detector noise plus the expected spikes due to cosmic rays hitting the detectors. These events occurred approximately once every 10 s per detector on average at float altitude. Because the events are uncorrelated with the chop, the events do not contribute to the demodulated signals but do increase the noise level.

We have not attempted to develop a detailed model for the cosmic-ray pulse height spectra observed on the bolometers. Instead, we give a phenomenalogical description drawn from a review by Simpson (1983), and a book by Longair (1986). Protons are the dominant fractional constituent (0.9) of cosmic-ray particles in the interstellar medium. At latitudes near 40°, the Earth's magnetic field traps protons with kinetic energies below ~5 GeV. The resulting integrated cosmic-ray flux of primary protons with energies above 5 GeV is ~0.1–0.5 $(\mathrm{cm}^2\ \mathrm{sr\ s})^{-1}$ at altitudes above 30 km. Protons passing through matter will deposit a minimum ionization energy of 1–2 MeV $\mathrm{cm}^2\ \mathrm{g}^{-1}$, given by the Bethe-Bloch function. We thus expect a mean event rate of 0.05–0.25 Hz and a minimum energy deposition of 10–20 KeV in our bolometer substrates which have an area and a thickness of 0.16 cm^2 and 25 μm, respectively. An energy deposition of 20 KeV in the bolometers used for this experiment will produce transient temperature and voltage changes of ~100 μK and 5 μV, respectively. A small number of pulses below the minimum ionization estimate are expected from events which graze the edge of a substrate or perhaps from secondary photon events generated by proton interactions with the aluminum cryostat or gondola frame.

The cosmic-ray identification was possible because the data were sampled rapidly enough to resolve the pulse response of the detector and preamplifier. The pulse detection algorithm high-pass filtered each detector signal. The filter had a four pole high-pass cut off for frequencies below 20 Hz which removed any signal components due to the chopper motion. Cosmic-ray events were identified if the sample to sample gradient of the filtered detector signal exceeded a fixed threshold. The gradient threshold was typically set near the 500 nV level, referenced to the detectors, which was ~7 times the RMS scatter expected from detector noise $V_n \approx 10\ \mathrm{nV}/\sqrt{\mathrm{Hz}}$ and the 50 Hz bandwidth of the electronics. If a cosmic ray was identified, the data were marked as contaminated for the next 100 samples or 10.52 s. Full chopper cycles which contained data were deleted. The resulting detector noise level was measured to be within 20% of that measured in the laboratory and less than 10% of the data was found to be contained.

The fractional stability of the secondary mirror amplitude and zero position were both better than 2×10^{-3} half an hour after reaching float altitude. Unfortunately, after 5 hours at float altitude, the chopper amplitude decreased because the motor bearings gradually froze due to improper lubrication. This limited the sensitivity of the instrument near the end of the flight.

The responsivity of the system was measured several times during the flight. The data were demodulated by multiplying by a square wave reference. The measured scatter in the demodulated bolometer cycles averaged over a 1 s period is used as an estimate of the short-term system noise. The chopped sensitivity is calculated as the ratio of the short-term noise to the measured responsivity. The measured chopped sensitivities of the four bands are given in Table 3.

The membrane calibration method assumes that the same fraction of the beam throughput which is intercepted at the prime focus by the membrane would be intercepted by a source filling half the sky. This can be tested by comparing the signal from the calibrator to the signal from a planet. If the size and temperature of the planet and the telescope beam shape are known, then one can calculate the fraction of the beam filled by the planet and thus the expected signal. During the first flight, the telescope scanned across Venus at an elevation of 11° above the horizon. The angular diameter of Venus on 1989 November 16 was $d_{\mathrm{Venus}} = 27''.4$. The effective antenna temperature of Venus is estimated from the measurements of Ulich

TABLE 3

MEASURED SENSITIVITY

BAND CENTER (cm^{-1})	SENSITIVITY ($\mathrm{mK_{CMB}}/\sqrt{\mathrm{Hz}}$)		
	1989 Nov[a]	1989 Nov[b]	1990 Jul[c]
3	17	19	(removed)
6	2.8	3.3	0.92
9	8.0	9.3	0.99
12	10	12	7.6

[a] Responsivity measured with membrane calibrator during first flight of 1989 November.

[b] Responsivity measured with scan across Venus during first flight of 1989 November.

[c] Responsivity measured with membrane calibrator during second flight of 1990 July.

(1981) and Whitcomb et al. (1979) to be 365, 300, 290, and 275 K in the 3, 6, 9, and 12 cm^{-1} bands. The sensitivity of each band, calculated from the scan of Venus, is listed in Table 3 and is within 20% of that derived from the membrane calibration.

The demodulated detector signals in all four bands had a small offset level of 1–2 mK_{RJ} for much of the flight. During the first flight we tested the dependence of the offset signals on the telescope elevation. We found that the offset signals vary in rough proportion to cosecant of the elevation angle θ. The factors of proportionality are 0.14, 0.23, and 0.43 [$mK_{RJ}/\sin(\theta)$] in the 6, 9, and 12 cm^{-1} bands, respectively. The elevation dependence of the offset in the 3 cm^{-1} band was not measurable. This spectrum increases more steeply than Raleigh-Jeans at higher frequencies but is not as steep as the predicted atmospheric emission for these bands. It is possible that the observed dependence is due to a combination of atmosphere and diffracted Earthshine.

The second flight was launched from the NSBF facility at Palestine, Texas, at 1:40 UT on 1990 July 2. The instrument was modified by the removal of the 3 cm^{-1} band and the substitution of improved bolometers into the 6 and 9 cm^{-1} bands. The package weight, balloon volume, float altitude, and flight duration were essentially the same as the first flight. Astrophysical observations during the second flight were limited to a 1.3 hr search for anisotropy in the CMB by a software problem that affected the telescope pointing system. The data from the second flight were demodulated by multiplying by a sinusoidal reference which reduces the response to high-frequency noise near odd harmonics of the chopper frequency. Further tests were made for systematic sources of noise in the demodulated detector signals.

The chopped sensitivities of the instrument were measured during the second flight and are listed in Table 3. The sensitivities of the 6 and 9 cm^{-1} bands were improved, over the first flight, by factors of 3 and 7, respectively. The responsivity was stable to 3% during the time at float altitude. The fractional stability of the secondary mirror amplitude and zero position were 4×10^{-4} and 2×10^{-3}, respectively.

In the 1990 July flight the demodulated detector signals had offsets of 5–7 mK_{RJ}. These offsets were not as stable as those during the first flight as is shown in Figure 10. In order to identify the source of the offset drifts we have measured the relative amplitude of the drifting component in each band. We find the spectrum of the amplitudes to be steeper than Raleigh-Jeans and to be roughly consistent with the calculated spectrum of ozone emission integrated over our filter bands. Another, less likely, possibility is that Earthshine accepted in an unmeasured sidelobe which has higher response at high frequencies could produce this signature. Fortunately, the time scale of the drifts is significantly longer than the 20 s time scale for pointed integrations in the scan of azimuthal position. This allows us to high pass filter the data to remove the long-term drifts while preserving sensitivity to spatial structure on angular scale up to 5° (Alsop et al. 1991b).

The measured Raleigh-Jeans offset signals in all bands are roughly proportional to the secondary mirror amplitude and zero position with coefficients of proportionality of 1 and 5 mK_{RJ}/degree, respectively. The zero position coefficient and the measured stability of the zero position imply that there should be drifts in the offset signals of 30 μK_{RJ} rms on the time scale of 3 s. This is close to the level of sensitivity which can be reached in a 20 s integration in the 9 cm^{-1} band which is the band most sensitive to changes in the temperature of a Raleigh-Jeans source. Data analysis has shown that the secondary mirror amplitude and zero position do not correlate with the scan position on the sky and therefore that these drifts will integrate away as a small additional source of noise.

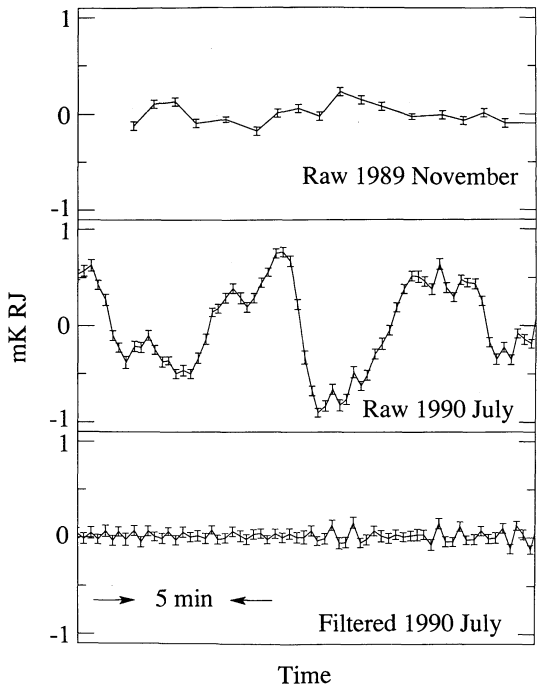

FIG. 10.—Comparison of offset drifts in the 12 cm^{-1} band measured during the 1989 November and 1990 July flights. The third graph shows the offset signal from the 1990 July flight after being filtered to remove the long-term drifts. The filtered data retain sensitivity to spatial structure on angular scales up to 5°.

Based on the encouraging results of the first two flights a third flight was conducted on 1991 June 4 from Palestine Texas at an altitude of 35 km to reduce the atmospheric emission. The instrument was improved with new dichroic filters to increase the optical efficiency and the high-frequency blocking. The analysis of data from the third flight is in progress.

We would like to thank Casey Inman, Albion Lawrence, Fred Rieke, Jeff Schuster, and Thor Wilbanks who each contributed to different stages of the project. We were fortunate to have the support of the machine and electrical shops in Berkeley and Santa Barbara. We also gratefully acknowledge the assistance of the staff of the National Scientific Balloon Facility.

M. L. F., D. C. A., and P. R. M. were partially supported by NASA Graduate Student Research Program Fellowships. Work at the University of California at Berkeley was funded by NASA grant NSG-7205 through the Space Sciences Laboratory, and by the Center for Particle Astrophysics, a National Science Foundation Science and Technology Center operated by the University of California under Cooperative Agreement No. AST-8809616. Work at the University of California at Santa Barbara was funded by NASA grant NAGW-1062, and the NSF's Center for Particle Astrophysics.

REFERENCES

Afsar, M. N. 1987, IEEE Trans. Instr. Meas., IM-36, 530
Alsop, D. C., et al. 1992a, in Trends in Particle Astrophysics (Singapore: World Scientific), in press
Alsop, D. C., et al. 1992, in preparation
Bond, J. R. 1989, in From Colliders to Cosmology, ed. A. Astbury & F. C. Khanna (Singapore: World Scientific)
Boughn, S. P., Cheng, E. S., Cottingham, D. A., & Fixen, D. J. 1992, ApJL, submitted
Chingcuarico, A. O., Lubin, P. M., Meinhold, P. R., & Tomizuka, M. 1991, Internat. J. Adaptive Control and Signal Proc., 5, 107
Fischer, M. L., et al. 1991, in AIP Conf. Proc. 222, After the First Three Minutes, ed. S. S. Holt, C. L. Bennet, & V. Trimble (New York: AIP), 123
Goody, R. M. 1964, Atmospheric Radiation, Vol. 1. (Oxford Univ. Press)
Gush, H. P., Halpern, M., & Wishnow, E. H. 1990, Phys. Rev. Lett., 65, 537
Haller, E. E. 1985, Infrared Phys., 25, 257
Hauser, M. G., et al. 1984, ApJ, 278, L15
Lange, A. E., Kreysa, E., McBride, S. E., Richards, P. L., & Haller, E. E. 1983, Int. J. Infrared Millimeter Waves, 4, 689
Longair, M. S. 1986, High Energy Astrophysics (Cambridge Univ. Press)
Lubin, P. M., Meinhold, P. R., & Chingcuanco, A. O. 1990, in The Cosmic Background Radiation 25 Years Later, ed. N. Mandolesi & N. Vittorio (Dordrecht: Kluwer)
Mather, J. C. 1981, IEEE Trans. Antennas Prop., AP-29, 967
Mather, J. C., et al. 1990, ApJ, 357, L37
Meinhold, P. R., & Lubin, P. M. 1991, ApJ, 370, L11
Meinhold, P. R., et al. 1992, in preparation
Meyer, S. S., Cheng, E. S., & Page, L. A. 1991, ApJ, 371, L7
Page, L. A., Cheng, E. S., & Meyer, S. S. 1990, ApJ, 355, L1
Readhead, A. C. S., Lawrence, C. R., Myers, S. T., Hardebeck, H. E., & Moffet, A. T. 1989, ApJ, 346, 556
Sato, S., Hayakawa, S., Lange, A. E., Matsumoto, T., Matsuo, H., Murakami, H., & Richards, P. L. 1987, Appl. Optics, 26, 410
Sato, S., Hayakawa, S., Matsumoto, T., Matsuo, H., Murakami, H., Sakai, K., Lange, A. E., & Richards, P. L. 1989, Appl. Opt., 28, 4478
Simpson, J. A. 1983, Ann. Rev. Nucl. Part. Phys., 33, 323
Smoot, G. F., et al. 1991, ApJ, 371, 1
Timusk, T., & Richards, P. L. 1981, Appl. Opt., 20, 1355
Ulich, B. L. 1981, ApJ, 86, 1619
Weiss, R. 1980, ARA&A, 18, 489
Whitcomb, S. E., Hildebrand, R. H., Keene, J., Stiening, R. F., & Harper, D. A. 1979, Icarus, 38, 75
Winston, R. 1970, Appl. Optics, 26, 245
Woody, D. P. 1975, Ph.D. thesis, Univ. of California at Berkeley